Journal of Hazardous Materials 219–220 (2012) 19–25

Contents lists available at SciVerse ScienceDirect

Journal of Hazardous Materials

journal homepage: www.elsevier.com/locate/jhazmat

Visible light CrO_4^{2-} reduction using the new $CuAlO_2$/CdS hetero-system

R. Brahimi[a,b], Y. Bessekhouad[b,c], N. Nasrallah[b], M. Trari[b,*]

[a] Centre of Research in Physical and Chemical Analysis (CRAPC), BP 248, RP 16004 Algiers, Algeria
[b] Laboratory of Storage and Valorization of Renewable Energies, Faculty of Chemistry (USTHB), BP 32 16111 Algiers, Algeria
[c] National Veterinary High School, BP 16111 Algiers, Algeria

ARTICLE INFO

Article history:
Received 27 July 2011
Received in revised form 5 March 2012
Accepted 6 March 2012
Available online 23 March 2012

Keywords:
Chromate
Delafossite
Hetero-system
Photo electrochemical

ABSTRACT

In this study, 64% of hexavalent chromium Cr(VI) reduction from the initial concentration (10^{-4} M) is reported under visible light using the ($CuAlO_2$/CdS) hetero-system. In this new hetero-system, low doped $CuAlO_2$ delafossite, synthesized by sol–gel works as an electrons reservoir with a wide space charge region (440 nm). In this case, the electron transfer to chromate is mediated via the hexagonal CdS variety, whose conduction band level is at −1.08 V with respect to the saturated calomel electrode which is more negative than the CrO_4^{2-}/Cr^{3+} level. This high reduction rate is achieved under optimized pH and $CuAlO_2$ percentage. Moreover, salicylic acid gives the best performance among hole scavengers and $CuAlO_2$ approaches 100% photostability at pH 7.5. The photo-catalytic process follows a pseudo first order kinetic with a half life of 2 h. The reaction products are identified by UV–visible spectrophotometry and linear voltametry at a platinum rotating electrode. The results reveal the presence of Cr^{3+} after irradiation.

1. Introduction

During the past decade, a great deal of attention has been paid to the use of photoelectrochemistry for purposes other than photovoltaic devices [1] and photochemical water splitting [2,3]. More specifically, its use for environmental protection applications [4,5]. For such applications, hexavalent chromium (Cr(VI)), which is present through the food chain is highly toxic, carcinogenic and tends to accumulate in living organisms. It is usually introduced in the effluents through industrial activities such as electroplating, leather tanning, dyes and chemicals manufacturing [6,7]. It is released in large amounts either as CrO_4^{2-} or $HCrO_4^-$ which, according to the potential–pH diagram, are thermodynamically stable species in water. Its persistence and its high solubility contribute to a large extent to the aquatic pollution and must be treated at the source. The conventional techniques for its elimination, such as reverse osmosis and the membranes techniques, are expensive, difficult to handle and do not often reach the level required by the world health organization guidelines. Such factors limit the threshold concentration of Cr(VI) at 0.5 mg L^{-1}.

As a result, new processes based on cheap equipments with high removal capability must be developed. To this end, photocatalysis has been widely used to remove heavy metals from wastewaters [8,9], and to mineralize hazardous organic compounds [10]. The Cr(VI) photo reduction into less harmful trivalent state has been reported over simple oxides because of the solar energy contribution to the environmental remediation [11]. In addition, Cr^{3+} is less toxic and can be readily precipitated as hydroxide or adsorbed onto various substrates. However, most semiconductor (SC) oxides absorb in the UV region and the large optical gap (Eg) makes them inefficient for the solar conversion despite their chemical stability [12]. Moreover, the energetic position of the valence band (VB) of O^{2-}: 2p character does not span the redox levels in solution [13]. The use of the narrow band gap SCs, on the other hand, makes the application of external polarization unavoidable, there by leading to a decrease of photoelectrochemical (PEC) efficiencies.

To mitigate these problems, considerable effort has been made in the development of optically active materials with new band structures. For example, $CuMO_2$ delafossites, where M is commonly a trivalent metal, have received renewed interest because of their optical gap, which is close to the ideal value required for terrestrial applications [14]. In addition, the electronic bands are made up of Cu-3d orbital, and the decrease of the gap occurs at the expense of valence band (VB) change toward higher energies. The lower filled t_{2g} level provides VB whereas the conduction band (CB) consists of empty hybridized dz_2/4s and the optical transition has a *d–d* characteristic. Accordingly, CB has a high reducing ability and the photoelectrons can reduce almost any kind of inorganic pollutant. We have previously tested their applicability in the metal deposition [4], hydrogen formation [15] and more recently in the environmental protection [8].

* Corresponding author. Tel.: +213 21 24 79 55; fax: +213 21 24 80 08.
E-mail address: solarchemistry@gmail.com (M. Trari).

0304-3894/$ – see front matter © 2012 Published by Elsevier B.V.
doi:10.1016/j.jhazmat.2012.03.011

Among the congeners, $CuAlO_2$ is a good candidate as photosensitizer because it is non toxic, chemical stable[1] and inexpensive. Moreover, its cage like framework is suitable to accommodate oxygen giving rise to *p* type conduction [16]. The potential of $CuAlO_2$-CB is more negative than the Cr(VI) level and should lead to a spontaneous reduction. However, the difference exceeds 1 V and the activity is weak. To overcome this drawback, some alternatives have been attempted and our investigations have been oriented toward the use of hetero-systems [16].

The life time of the charge carriers in $CuAlO_2$ is short because of the low mobility, and the photoactivity is dependent on the initial preparation conditions. The sol–gel requires relatively low temperatures and should lead to high quantum yields by decreasing the crystallite size i.e., the distance the electrons have to diffuse before reaching the interface. The use of CdS is now well accepted as mediator in photoredox reactions [17]. Due to its large band gap (2.4 eV), CdS can be used as a bridge for the electron transfer in heterogeneous catalysis. The electrons in $CuAlO_2$-CB can thus be injected into CdS-CB, which in turn cause the Cr(VI) reduction. Nevertheless, the question of longevity still remains open and a chemical photostability is required for long term applications. The PEC process is enhanced in presence of holes scavenger which competes with the photo corrosion; salicylic acid (SA) being particularly favorable. Preliminary tests have shown a good stability above pH 7. The current study investigates the synthesis of $CuAlO_2$ by sol–gel, its PEC characterization and its application for the photocatalytic reduction of chromate over the hetero-system $CuAlO_2$/CdS.

2. Experimental procedures

$CuAlO_2$ is synthesized with a slightly modified preparation adopted previously [8]. CuO (Fluka 99%, dried at 400 °C) is dissolved in a minimum of HNO_3 (6 mol L^{-1}) and mixed to $Al(NO_3)_3{\cdot}9H_2O$ (Labosi > 99%) dissolved in 60 mL of ethylene glycol. The mixture is maintained 2 h at ambient temperature until total dissolution, and is then evaporated under reflux at 70 °C (6 h). Next, the mixture is dehydrated at 120 °C and denitrified on a magnetic stirring hot plate. The powder is then ground, pressed into pellets and treated at 1100 °C (150 °C h^{-1}). Finally, the sample is allowed to naturally cool down in the furnace. The process is repeated twice to get a single phase; the end product shows a blue color and the compactness approximates 80%.

On the other hand, CdS is prepared by hydrothermal route as follows. $CdSO_4{\cdot}8/3H_2O$ (Panreac 99%, 1 mmol) and thiourea $SC(NH_2)_2$ (Riedel de Haeïn, 99%, 1 mmol) are added to 40 mL of ethylenediamine. The aqueous solution is transfered into Teflon lined autoclave of 100 mL volume (filled at 80%) maintained for 12 days at 150 °C. The product is washed with water, ethanol and dried at 60 °C. The purity of the phases is checked by X-ray diffraction using a Phillips PW 1710 X-ray diffractometer with a copper anticathode (λ = 0.154178 nm). The data are collected with a step of 0.1° (2θ) min^{-1} over the angular range (10–90°). The crystallite size is evaluated from the full width at half maximum (FWHM). The crystallites size distribution is performed by laser-particle-size analysis (Mastersizer 2000, Malvern). The specific surface area is determined from BET measurement with N_2 adsorption isotherms using micromeritics Accu 2100E.

Silver used as ohmic contact produces low resistances. The pellet is assembled in a glass holder using epoxy resin, leaving an exposed area of 0.5 cm^2. The electrochemical measurements are done in a three compartment cell filled with Na_2SO_4 (0.1 mol L^{-1}). A Pt sheet (1 cm^2) and a saturated calomel electrode (SCE) are used as auxiliary and reference electrodes respectively. The intensity–potential $J(E)$ curves are plotted with a PGZ301 potentiostat (radiometer analytical) at a scan rate of 10 mV s^{-1}. The Mott–Schottky characteristics are recorded at a frequency of 10 kHz. Such a frequency is high enough that the capacitance of the space charge region dominates. Due to the dielectric constant (~35 at 10 kHz), the approximation $C_H \gg C_{sc}$ is valid and the term $(1/C_H)$ can be neglected. The working electrodes ($CuAlO_2$ and CdS) are illuminated with a tungsten lamp (200 W) emitting in the range 400–800 nm.

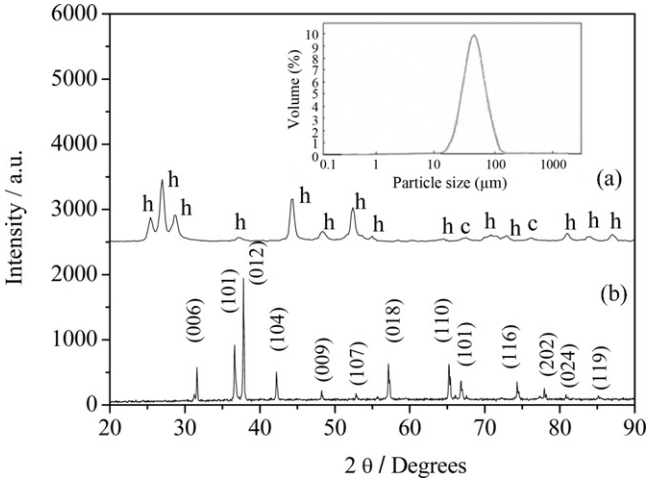

Fig. 1. XRD patterns of (a) CdS and (b) $CuAlO_2$. (Inset) the particle size distribution of CdS.

The photocatalytic Cr(VI) reduction is carried out in an aerated ($CuAlO_2$(*x*%)/CdS) dispersion in a double walled Pyrex reactor. The solubility of SA is fixed at 10^{-4} mol L^{-1} and the pH is maintained at 7.5 by adding NaOH. The mixture is sonicated before illumination for 3 min with a digital ultrasonic cleaner (WiseClean Wisd 23) to obtain highly dispersed catalyst. The temperature is regulated at 30 ± 1 °C with a thermostated bath (Julabo) and the solution is shaken by magnetic stirring. The visible illumination is provided by a 150 W halogen lamp whose primary radiation is emitted at 650 nm (8.3 mW cm^{-2}). The aliquots are regularly taken every 15 min and centrifuged to remove precipitates. The progress of the Cr(VI) reduction is followed by titration at 350 nm using UV–visible spectrophotometer (Shimadzu 1800). Potentiometric titration at a Pt rotating electrode (Radiometer analytical CVT 101T) is also used for Cr(VI) determination, the speed of agitation is maintained at 2000 rpm and the limiting current is measured using Pt wire (type EM EDI-PT). The oxidation of SA is monitored by measuring the absorbance at 298 nm. The water used throughout the experiments is distilled and all solutions are prepared from reagents of analytical quality. The Cd^{2+} concentration is determined after each run by atomic absorption (Perkin Elmer 2380).

3. Results and discussion

3.1. Characterization

The X-ray diffraction pattern (Fig. 1) reveals $CuAlO_2$ single phase with no secondary impurities like the spinel $CuAl_2O_4$. All peaks match those of the JCPDS card No. 12-1235 (SG : $R\bar{3}m$). The delafossite is a layered structure and the channels in the basal plans are large enough to host foreign ions [18]. The main doping comes from oxygen intercalation which leads to *p*-type conductivity, giving the opportunity to characterize the oxide photoelectrochemically. In addition, $CuAlO_2$ shows a chemical stability over the whole pH range. The position of the bands under the working conditions

[1] $CuAlO_2$ is stable over the whole pH range and does not dissolve enven in aqua-regia and perchloric acid.

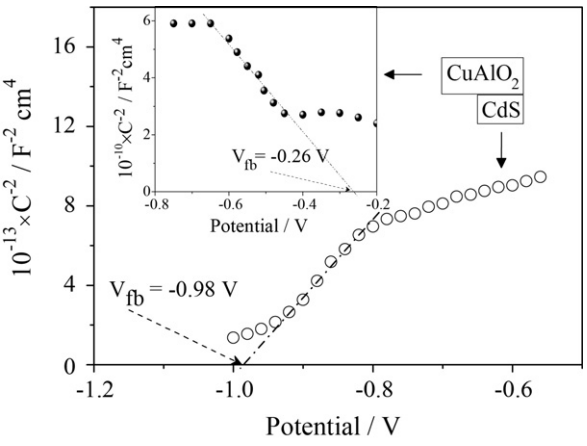

Fig. 2. The Mott–Schottky characteristics of CdS and $CuAlO_2$ (inset).

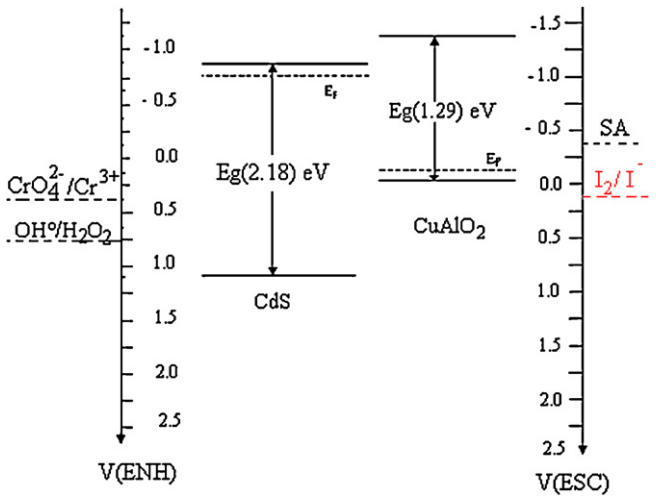

Fig. 3. The energy band diagram of CdS/$CuAlO_2$ hetero-junction in presence of hole scavengers.

is determined from the capacitance measurement. The flat band potential V_{fb} (−0.26 V) and the holes density (1.49×10^{19} cm^{-3}) are respectively determined from the intercept of the potential-axis at $C^{-2} = 0$ and the slope of the linear part of the Mott–Schottky plot (Fig. 2):

$$\frac{1}{C^2} = \pm\frac{2}{e\varepsilon\varepsilon_0 S N_A}\left(E - E_{fb} - \frac{kT}{e}\right) \quad (1)$$

where S is the surface of the electrode and the other symbols have the usual meaning. The linear plot indicates a constant density N_A, which is a characteristic of lightly doped semiconductor with a wide depletion width (440 nm)[2]. The X-ray diffraction (Fig. 1) shows the main peaks of the hexagonal phase. CdS currently presents two crystallographic varieties. The positive slope of the Mott–Schottky plot indicates a *n*-type conduction characteristic where the dominant carriers are electrons.

The semiconductor is the key element of solar devices. With a band-gap of 1.29 eV [16], $CuAlO_2$ has the capability of converting more than 90% of the sunlight. The photoactivity is governed by the active surface of the powder. The small crystallites are advantageous in photocatalysis, particularly for low mobility polaron oxides by minimizing the distance the electrons have to diffuse to reach the interface. The crystallite size must be comparable with the minority-carriers-diffusion length. It, however, must exceed the penetration depth (α^{-1}) in order to collect most (e^-/h^+) pairs, α being the optical absorption coefficient (~10 cm^{-1}). Our strategy is, therefore, to prepare the oxide in nano crystalline morphology of the kind already obtained with $CuFeO_2$ [8]. The oxide is elaborated from the nitrates decomposition which has the advantage of producing submicron-sized particles with narrow particle size distribution (Fig. 1, inset). The crystallite size of $CuAlO_2$ (43 nm) is determined from FWHM: $L = 0.94\lambda/\beta\cos(\theta)$, where β (rd.) is the broadening of the most intense XRD peak (0 1 2). The size of CdS calculated using the same procedure averages 13 nm. Assuming spherical and non porous crystallites (Fig. 1 inset), such value leads to a specific surface of 95 m^2 g^{-1} $\{=6(\rho L)^{-1}\}$, which is close to that determined from BET (~80 m^2 g^{-1}).

3.2. Photocatalysis

3.2.1. $CuAlO_2$

The *p*-$CuAlO_2/CrO_4^{2-}$ junction is sufficiently depleted to exclude the recombination of (e^-/h^+) pairs and the system has a strong driving force to reduce chromate into trivalent state. However, the performance of oxides is limited and more efficient systems are required. Indeed, the heterogeneous charge transfer at the SC/electrolyte interface should occur iso-energetically and the large difference ($V_{CB} - E_{red} \sim 1$ V) makes the photoactivity weak where only 3% of CrO_4^{2-} is reduced. Accordingly, an optimal band bending of ~0.5 V is required for a charge separation as previously claimed by Gerisher [19]. The hetero-system is an attractive way to enhance the photoactivity. In this case, the performance can be explained by invoking mediation of wide band gap SC in the charge transfer which mainly occurs by collision [20]. The current matching is determined by the relative positions of the band edges leading to cascade PEC cell. Our group has previously reported some improvement with the $CuAlO_2/TiO_2$ system [16]. CdS absorbs wavelengths greater than 565 nm and is experimented in an attempt to shift its spectral response toward lower energies. The energy band diagram (Fig. 3) shows that the interfacial electron transfer is achieved by injection from $CuAlO_2$ to CdS. Such process has been clearly demonstrated when using a band pass filter ($\lambda > 600$ nm).

The dark adsorption is a precondition for the photocatalysis, CdS has the dual role of an adsorbat and an electron bridge. The point of zero charge (pzc), i.e., pH at which the adsorbed surface is zero, is found to be 6.6. At pH ~7.5, the CrO_4^{2-} species predominate ($HCrO_4^- \leftrightarrow CrO_4^{2-} + H^+$, $pK_a = 6.49$ [21]) and are attracted by the positively charged CdS surface. The CdS free potential (−0.302 V) and the equilibrium time (~20 min) are determined from the chrono-potentiometric profile of the $CuAlO_2/CdS/CrO_4^{2-}$ suspension. The chromate reduction increases when the $CuAlO_2$ amount in the ($CuAlO_2(x)$)/CdS hetero-system is increased and reaches a maximum for $x = 25\%$, above which a regression in the activity is observed (Fig. 4). The high performance is attributed to the increase of the catalyst amount in which each particle, reached by incident photons, participates in the generation of charge carriers and there by the reduction process. The excess of the catalyst (beyond 25%) acts as a light filter, thus decreasing the photons flux. The shadowing effect and the turbidity of the solution also account for the photo-activity the regression.

3.2.2. Hole scavengers

Like most oxides, $CuAlO_2$ does not undergo a photo-corrosion when a suitable hole scavenger is used. This fact is illustrated in the efficiency over ($CuAlO_2$(25%)/CdS). The chromate reduction in presence of SA (64%) is better than with hydrogen peroxide, iodide

[2] Calculated from the relation $(e\varepsilon\varepsilon_o \Delta V/eN_A)^{0.5}$, ΔV (= 0.5 V) is the optimal band bending at the interface.

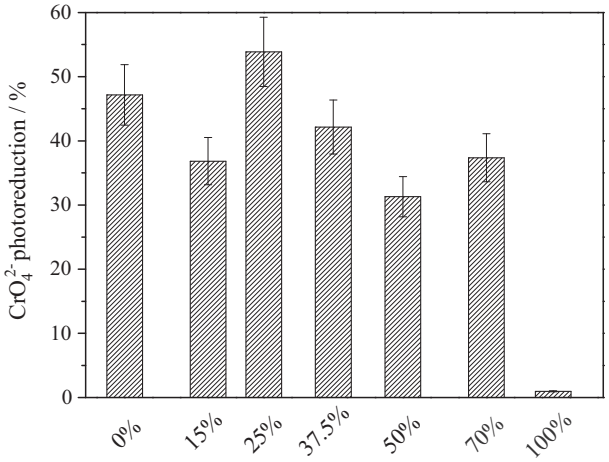

Fig. 4. Photocatalytic reduction of CrO_4^{2-} as function of $CuAlO_2$ mass in the heterojunction: $CuAlO_2$(wt%)/CdS (125 mg), CrO_4^{2-}, 10^{-4} mol L^{-1} at neutral pH.

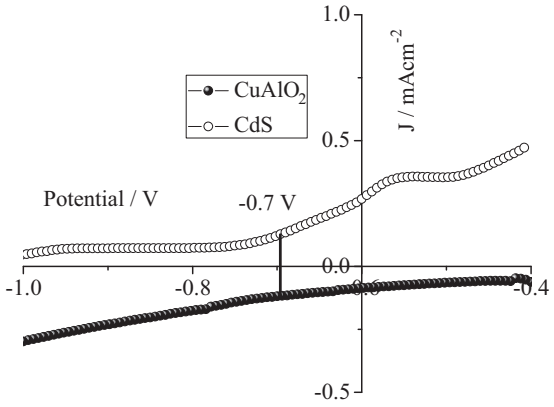

Fig. 6. *J–E* curves of CdS and $CuAlO_2$ electrodes in Na_2SO_4 solution.

and oxalic acid under similar conditions (Fig. 5). It is worthwhile to outline that the potential of the I_2/I^- couple is more anodic than the $CuAlO_2$-VB and does not react with photoholes. The redox potential of SA is not available in the literature and is determined by plotting the *J*(*E*)curve in the working solution (Fig. 5 inset). The peak (approx. −0.3 V) located below the $CuAlO_2$-VB indicates a spontaneous oxidation through holes process, thus providing a good protection against photo-corrosion. Assuming a total mineralization, the reaction can be written as follows:

$$4CrO_4^{2-} + 3\,C_7H_6O_3 + 18O_2 + 20H^+ \rightarrow 4Cr^{3+} + 21CO_2 + 19H_2O \quad (2)$$

with a negative free enthalpy [21] and a spatial separation of two half electrochemical reactions. Reaction (2) is thermodynamically feasible but requires a large over-potential and the light could be used for this purpose. One can derive the power characteristic from the separate *J*(*E*) curves of *n*-CdS and *p*-$CuAlO_2$ plotted in the same scale (Fig. 6). The hetero-system is in a short circuited configuration with a negligible electrolytic resistance. The equilibrium potential (−0.69 V) is obtained by connecting the points of equal intensities.

The presence of oxygen (Reaction (2)) contributes significantly to the photocatalytic process. Indeed, the percentage of CrO_4^{2-} reduced under nitrogen bubbling decreases by 33% (Fig. 8b). The photoreduction reaches a saturation after ∼2 h and further illumination decreases only slightly the Cr(VI) concentration. As the concentration of CrO_4^{2-} decreases, the reaction involving H_3O^+ ion becomes predominant and most electrons go to hydrogen production, which explains the tendency to saturation [22]. The absorption spectra are presented in Fig. 7, λ_{max} slightly shifts to longer wavelengths (350–375 nm), which is caused by the complex formation between Cr(VI) and SA. Similar results have already been observed with the same species on TiO_2 [23]. In this case, Cr^{3+} cannot be easily detected by spectrophotometry because it interferes with SA (λ_{max} = 298 nm). In order to confirm the presence of Cr^{3+}, we have analyzed the aliquots by potentiometry at a rotating Pt disc and the results are reported in Fig. 8a. The reactants in a mixture behave independently from one another when the half potentials differ by at least 0.2 V.

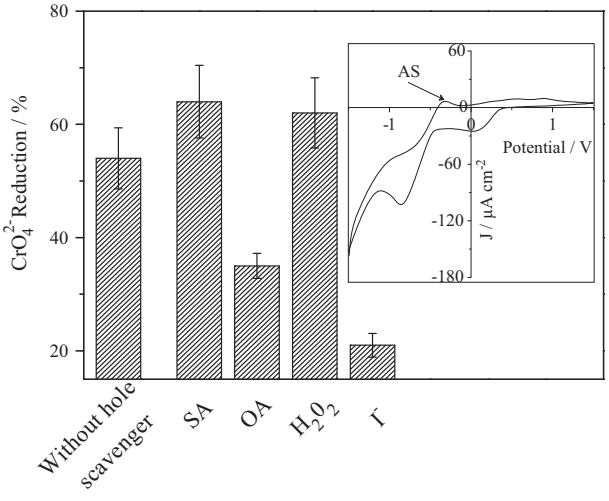

Fig. 5. Effect of hole scavenger on the photoreduction of CrO_4^{2-}. (Inset) The *J–E* curves of SA at neutral pH.

3.2.3. Chromate concentration

3.2.3.1. Chromate adsorption. The chromate reduction follows a Langmuir adsorption isotherm and is dependent on the initial concentration (C_o). The adsorption capacity at equilibrium (Q_{ads}) is given by:

$$Q_{ads} = \frac{(C_o - C_e)V}{m} \quad (3)$$

where C_e is the equilibrium concentration of the adsorbate (mg L^{-1}), *V* is the volume of the solution (L), and m is the mass of the catalyst (g). Q_{ads} is determined from the equation:

$$\frac{C_e}{Q_{ads}} = \frac{C_e}{Q_m} + \frac{1}{K_{ads}Q_m} \quad (4)$$

where Q_m and K_{ads} are the maximum adsorption and the specific adsorption of CrO_4^{2-} respectively (Fig. 9).

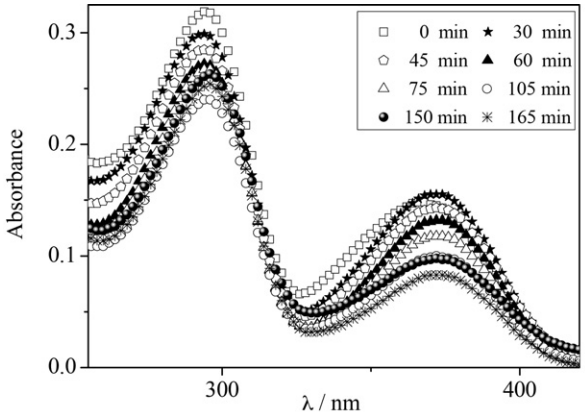

Fig. 7. UV–visible spectra of CrO_4^{2-} in presence of SA (at pH ∼4) in an aerated solution.

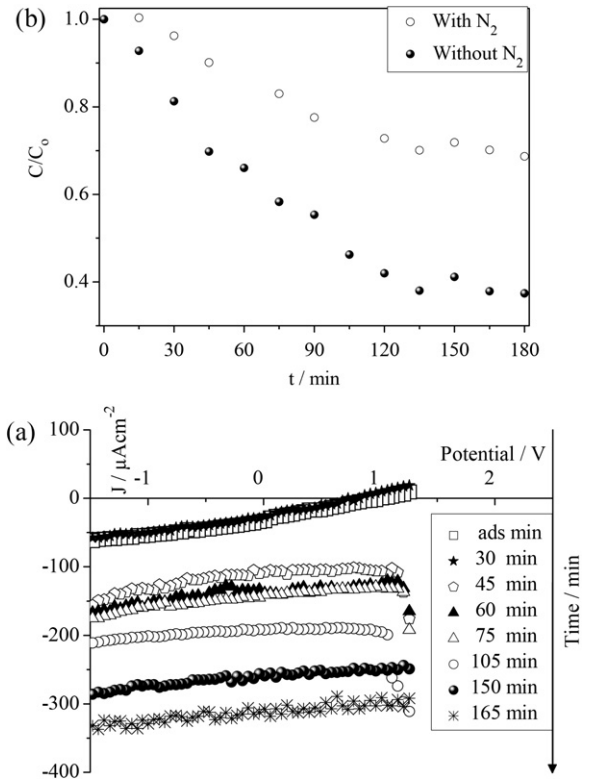

Fig. 8. (a) The *J–E* curves of the CrO_4^{2-} reduced into Cr^{3+} as function of time (at pH ~4) using a rotating Pt disc (2000 rpm) without N_2 bubbling. (b) The same reaction under nitrogen bubbling.

3.2.3.2. Kinetic of the chromium reduction. The effect of the C_o concentration on the photo activity is investigated at neutral pH with the best configuration i.e., $CuAlO_2$ (25%)/CdS (Fig. 10a). The performance decreases with increasing C_o and the chromate excess induces a drawback effect, which is a consequence of the optical filter generated by CrO_4^{2-} itself that absorbs in the visible region. The second reason is due to Cr^{3+} generation which precipitates as $Cr(OH)_3$ ($k_s \times 10^{-31}$), occupying active sites by covering the catalyst surface. The absence of peak at 305 nm (ascribed to Cr^{3+}) in the UV–visible spectrum of the 3-h-illuminated solution further support this hypothesis. The apparent constant k_{app} is dependent on C_o and the chromate reduction is well described

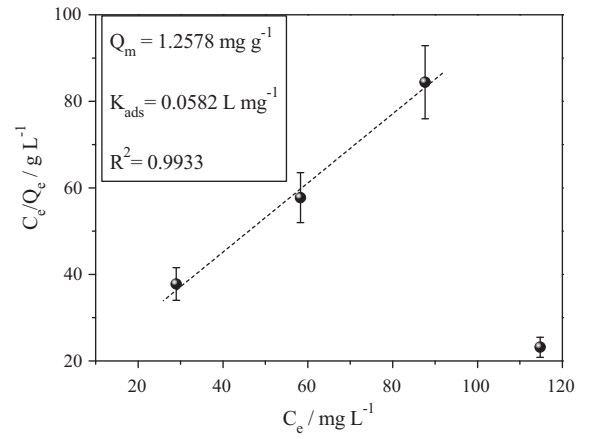

Fig. 9. The Langmuir adsorption isotherm (see the text for the symbols). Pseudo-first order kinetic for CrO_4^{2-} photoreduction for various concentrations.

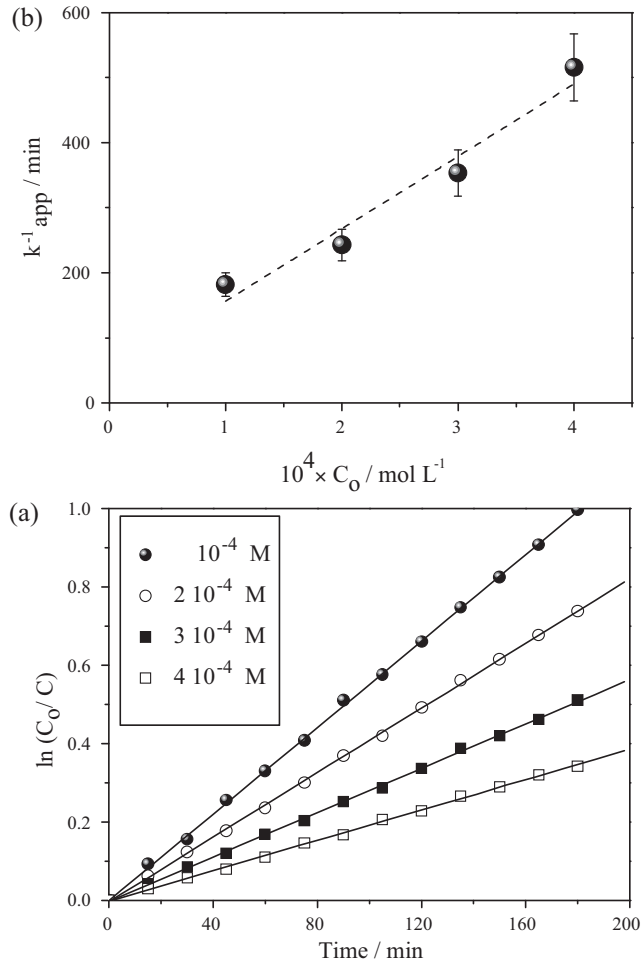

Fig. 10. (a) Pseudo-first order kinetic for CrO_4^{2-} photoreduction for various concentrations. (b) The apparent rate constants.

by the Langmuir–Hinshelwood model at concentrations less than 3×10^{-4} mol L^{-1} [24]:

$$-\frac{dC}{dt} = k_{app} C_o \quad (5)$$

The plot of k_{app}^{-1} versus C_o (Fig. 10b) allows the evaluation of both the rate constant k_r (2.64×10^{-4} min^{-1} g L^{-1}) and the adsorption constant k_s (83.9 L g^{-1}):

$$\frac{1}{k_{app}} = \frac{1}{k_r k_s} + \frac{C_o}{k_r} \quad (6)$$

The kinetic parameters are gathered in Table 1 along with the correlation coefficients (R^2) and the half life times ($t_{1/2}$).

3.2.4. pH

The chemical stability is a crucial factor for long term applications. Thus, the question that arises is to know whether CdS is

Table 1
The apparent pseudo first order rate constant, correlation coefficient and half life on various concentrations for chromate photoreduction.

$10^4 \times C_o$ (mol L^{-1})	$10^4 \times k_{app}$ (min^{-1})	t (min)	k_r (min^{-1} g L^{-1})	k_s (L g^{-1})
1	55	126	2.64×10^{-4}	83.9
2	41	169		
3	28	247		
4	19	365		

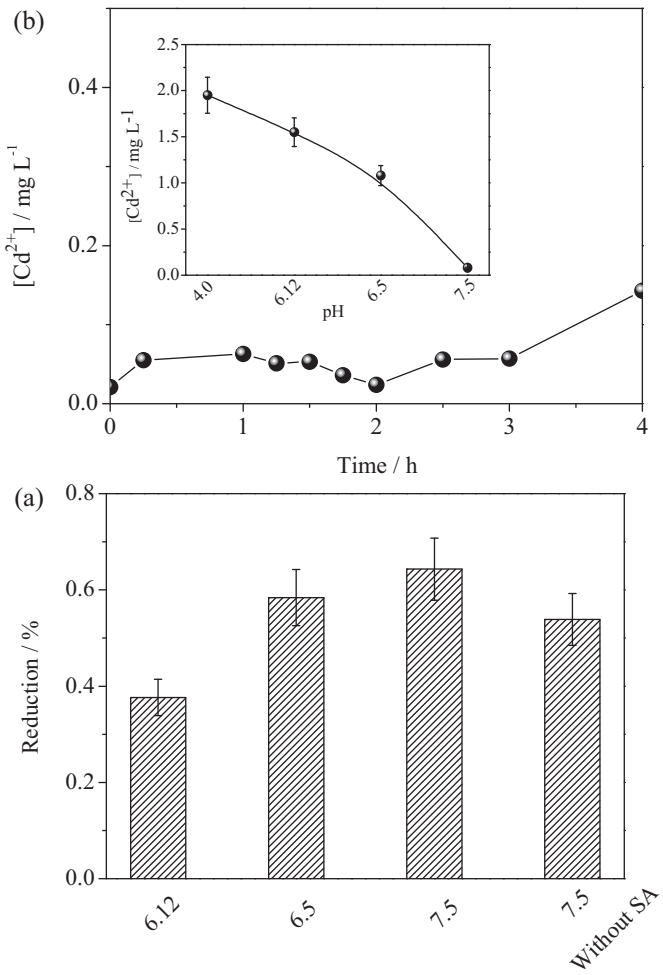

Fig. 11. (a) The effect of pH toward the CrO_4^{2-} photoreduction. (b) Cd^{2+} concentration as function the time and the pH.

stable under the operating conditions. Up to one week of immersion in the working solution, there has not been any degradation in the dark, the amount of Cd^{2+} titrated by atomic absorption is less than the experimental error. Under illumination, however, the corrosion rate increases with decreasing pH (Fig. 11b). Such situation has also been observed by others [17]. However, at pH ~7.5, close to that of the natural aquatic environment, CdS shows a good chemical stability up to 4 h of continuous illumination.

Both $CuAlO_2$ and CdS have electronic bands that are pH-insensitive and a variation of pH does not change significantly the band bending at the solid interface. By contrast, the potential of CrO_4^{2-} varies by $-0.16\,V\ pH^{-1}$ and one would have the further advantage to move appropriately the CrO_4^{2-}/Cr^{3+} level with respect to CdS-CB by working at neutral pH (Fig. 11a). In addition, such pH shifts cathodically the potential of the CrO_4^{2-}/Cr^{3+} pair, which favors the charge separation and in this way the photo activity.

4. Conclusion

In this study, 64% reduction of hexavalent chromium (Cr(VI)) is achieved under mild conditions using a suspension of the $CuAlO_2$(25%)/CdS hetero-system. $CuAlO_2$ is chosen as photosensitizer because of its corrosiveness and low cost. It also possesses a high reducing ability due to *d*-character of the conduction band. $CuAlO_2$ was prepared by sol–gel with an increase of the surface/bulk ratio. In this case, the light doping provides a wide depletion layer which is advantageous for small polaron oxides. The photoactivity is due to the electron injection from the $CuAlO_2$-CB to the less cathodic CdS-CB. The merit of CdS lies in the pH-invariance of the electronic bands. This allows an adjustment of the CrO_4^{2-} level which, at pH 7.5, is appropriately positioned to mediate the electron transfer. Among hole scavengers, salicylic acid gives the best performance, which favors the charge separation and enables $CuAlO_2$ to be photoelectrochemically stable. The mineralization occurs through oxidative pathway by both photo holes and dissolved oxygen. The analysis of the final products is confirmed by both spectrophotometry and potentiometry.

Acknowledgments

The authors would like to thank B. Bellal for his technical assistance and valuable discussion. This work was supported financially by the Faculty of Chemistry (USTHB, Algiers).

References

[1] S. Pavasupree, Y. Suzuki, S. Pivsa-Art, S. Yoshikawa, Synthesis and characterization of nanoporous, nanorods, nanowires metal oxides, Sci. Technol. Adv. Mater. 6 (2005) 224–229.
[2] M. Ni, M.K.H. Leung, D.Y.C. Leung, K. Sumathy, A review and recent developments in photocatalytic water-splitting using TiO_2 for hydrogen production, Renew. Sust. Energy Rev. 11 (2007) 401–425.
[3] R. Brahimi, Y. Bessekhouad, A. Bouguelia, M. Trari, Visible light induced hydrogen evolution over the heterosystem Bi_2S_3/TiO_2, Catal. Today 122 (2007) 62–65.
[4] W. Ketir, A. Bouguelia, M. Trari, Photocatalytic removal of M^{2+} (=Ni^{2+}, Cu^{2+}, Zn^{2+}, Cd^{2+}, Hg^{2+} and Ag^{+}) over new catalyst $CuCrO_2$, J. Hazard. Mater. 158 (2008) 257–263.
[5] Y. Bessekhouad, N. Chaoui, M. Trzpit, N. Ghazzal, D. Robert, J.V. Weber, UV–vis versus visible degradation of acid orange II in a coupled CdS/TiO_2 semiconductors suspension, J. Photochem. Photobiol. A: Chem. 183 (2006) 218–224.
[6] Y. Gong, X. Liu, L. Huang, W. Chen, Stabilization of chromium: an alternative to make safe leathers, J. Hazard. Mater. 179 (2010) 540–544.
[7] M. Gheju, A. Lovi, I. Balcu, Hexavalent chromium reduction with scrap iron in continuous-flow system. Part 1. Effect of feed solution pH, J. Hazard. Mater. 153 (2008) 655–662.
[8] S. Bassaid, M. Chaib, S. Omeiri, A. Bouguelia, M. Trari, Photocatalytic reduction of cadmium over $CuFeO_2$ synthesized by sol–gel, J. Photochem. Photobiol. A: Chem. 201 (2009) 62–68.
[9] S. Omeiri, Y. Gabès, A. Bouguelia, M. Trari, Photoelectrochemical characterization of the delafossite $CuFeO_2$: application to removal of divalent metals ions, J. Electroanal. Chem. 614 (2008) 31–40.
[10] N. Serpone, P. Marathamuthu, P. Pichat, E. Pelizzetti, H. Hidaka, Exploiting the interparticle electron transfer process in the photocatalysed oxidation of phenol, 2-chlorophenol and pentachlorophenol: chemical evidence for electron and hole transfer between coupled semiconductors, J. Photochem. Photobiol. 85 (1995) 247–255.
[11] C.S. Uyguner, M. Bekbolet, Evaluation of humic acid, chromium (VI) and TiO_2 ternary system in relation to adsorptive interactions, Appl. Catal. B: Environ. 49 (2004) 267–275.
[12] J. Nowotny, C.C. Sorrell, T. Bak, L.R. Sheppard, Solar-hydrogen: unresolved problems in solid-state science in solid-state science, Sol. Energy 78 (2005) 593–602.
[13] U. Diebold, The surface science of titanium dioxide, Surf. Sci. Rep. 48 (2003) 53–229.
[14] S. Saadi, A. Bouguelia, H. Derbal, A. Aider, M. Trari, Hydrogen photoproduction over new catalyst $CuLaO_2$, J. Photochem. Photobiol. A 187 (2007) 97–104.
[15] M. Younsi, A. Bouguelia, A. Aider, M. Trari, Visible light-induced hydrogen over $CuFeO_2$ via $S_2O_3^{2-}$ oxidation, Sol. Energy 78 (2005) 574–580.
[16] R. Brahimi, Y. Bessekhouad, A. Bouguelia, M. Trari, $CuAlO_2/TiO_2$ heterojunction applied to visible light H_2 production, J. Photochem. Photobiol. A: Chem. 186 (2007) 242–247.
[17] A.H. Zyouda, N. Zaatara, I. Saadeddina, A. Cheknane, D. Parkc, G. Campetc, H.S. Hilal, CdS-sensitized TiO_2 in phenazopyridine photo-degradation: catalyst efficiency, stability and feasibility assessment, J. Hazard. Mater. 173 (2010) 318–325.
[18] T. Ishiguro, N. Ishizawa, N. Mizutani, M. Kato, High temperature structural investigation of the delafossite type compound $CuAlO_2$, J. Solid State Chem. 41 (1982) 132–137.
[19] Gerisher, Energy conversion with semiconductor electrodes, in: B.O. H. Seraphin (Ed.), Topics in Applied Physics, Solid State Physics Aspects, 1978.

[20] B. Bellal, B. Hadjarab, A. Bouguelia, M. Trari, Visible light photocatalytic reduction of water using $SrSnO_3$ sensitized by $CuFeO_2$, Theor. Exper. Chem. 45 (2009) 172–179.
[21] Handbook of chemistry and physics. 78th ed., Editor-in-Chief David R. Lide CRC Press, 1997–1998.
[22] R. Gherbi, N. Nasrallah, A. Amrane, R. Maachi, M. Trari, Photocatalytic reduction of Cr(VI) on the new hetero-system $CuAl_2O_4/TiO_2$, J. Hazard. Mater. 186 (2011) 1124–1130.
[23] G. Colón, M.C. Hidalgo, J.A. Navio, Influence of carboxylic acid on the photocatalytic reduction of Cr(VI) using commercial TiO_2, Langmiur 17 (2001) 7174–7180.
[24] Y. Li, S. Sun, M. Ma, Y. Ouyang, W. Yan, Kinetic study and model of the photocatalytic degradation of rhodamine B (RhB) content, light intensity and TiO_2 content in the catalyst, Chem. Eng. J. 142 (2008) 147–155.